Electronic Supporting Information

Water-soluble amphiphilic ruthenium(II) polypyridyl complexes as potential light-activated therapeutic agents

Sandra Estalayo-Adrián,*[ab] Salvador Blasco,[a] Sandra A. Bright,[c] Gavin J. McManus,[c] Guillermo Orellana,[d] D. Clive Williams,[c] John M. Kelly [a] and Thorfinnur Gunnlaugsson *[a]

[a]School of Chemistry and Trinity Biomedical Sciences Institute (TBSI), Trinity College Dublin, The University of Dublin, Dublin 2, Ireland. E-mail: estalays@tcd.ie, jmkelly@tcd.ie, gunnlaut@tcd.ie

[b]Advanced Materials and BioEngineering Research (AMBER) Centre, Trinity College Dublin, The University of Dublin, Dublin 2, Ireland

[c]School of Biochemistry and Immunology, Trinity Biomedical Sciences Institute (TBSI), Trinity College Dublin, The University of Dublin, Dublin 2, Ireland

[d]Department of Organic Chemistry, Faculty of Chemistry, Universidad Complutense de Madrid, E-28040 Madrid, Spain

---

Table of Contents **Page No**

Experimental Section

Materials

Chemicals and solvents: All chemicals were obtained from Sigma-Aldrich, TCI, Alfa Aesar or Fluorochem and, unless specified, were used without further purification. Chromatographic columns were run using Aluminium oxide neutral (Brockmann I) 60 Å (50–200 μm). Analytical thin layer chromatography (TLC) was performed on aluminium oxide neutral plates. Deuterated solvents for NMR use were purchased from Apollo Ltd. Solvents for synthetic purposes were used at general purpose reagent (GPR) grade unless otherwise stated. Dry solvents were obtained from a solvent purification system (SPS) purchased from Innovative Technology Inc. Phosphate-

buffered solutions were prepared by dilution of the appropriate amount of sodium monobasic and dibasic in ultrapure water (Millipore Milli-Q). The pH of the sodium phosphate-buffered aqueous solution was adjusted to 7.4 by addition of NaOH using a pH-meter.

Cell culture: HeLa cells were grown in a cell culture flask using Dulbecco's Modified Eagle Medium supplemented with 10% foetal bovine serum, 1% penicillin/streptomycin and 0.2% plasmocin at 37 °C in a humidified atmosphere with 5% CO_2.

General Experimental Apparatus and Techniques

Nuclear magnetic resonance (NMR) spectroscopy: All NMR spectra were recorded using either a Bruker Avance III 400 NMR spectrometer operating at 400 MHz for ^{1}H NMR and 101 MHz for ^{13}C NMR, or a Bruker Avance II 600 NMR spectrometer operating at 600 MHz for ^{1}H NMR and 151 MHz for ^{13}C NMR. Chemical shifts (δ) were referenced relative to the internal solvent signals. All NMR spectra were carried out at 25.0 °C.

Mass spectrometry: Electrospray ionisation (ESI) mass spectra were recorded on a Micromass LCT spectrometer calibrated against a leucine enkephalin (Tyr-Gly-Gly-Phe-Leu) standard (*m/z* = 556.2771). Matrix-assisted laser desorption/ionization (MALDI) mass spectra were recorded on a MALDI QToF Premier (Waters Corporation, Micromass MS Technologies, Manchester, UK) and high resolution (HR) mass spectra were determined by a peak matching method using Glu-Fib as an internal reference (*m/z* = 1570.677). All accurate mass values were reported within ±5 ppm.

Infrared spectroscopy: Infrared spectra were recorded on a Perkin Elmer Spectrum One FT-IR spectrometer fitted with a Universal ATR Sampling Accessory for solid samples.

Melting points: Melting points were determined using an IA9000 digital melting point apparatus.

Elemental analysis: Elemental analyses were conducted at the Microanalytical Laboratory, School of Chemistry, University College Dublin (UCD).

Microwave reactions: Reactions in which microwave irradiation was used were carried out using a Biotage® Initiator microwave synthesizer.

UV-vis absorption spectroscopy: UV-vis absorption spectra were recorded in a 1-cm Suprasil cuvette (3 mL) on a Varian CARY 50 spectrophotometer with a wavelength range of 200–900 nm and a scan rate of 600 nm min^{-1}. Baseline correction measurements were used for all spectra.

Absorption coefficients: Molar absorption coefficients were determined by measuring the absorption spectra of each ruthenium complex at different concentrations. The appropriate

absorption maxima (typically π-π^* IL and MLCT transitions) were plotted versus the Ru(II) complex concentration and the absorption coefficients were calculated from the slope of the linear regression line according to the Bouguer-Lambert-Beer law.

Luminescence spectroscopy: Luminescence measurements were performed in a 1-cm Suprasil cuvette (3 mL) on a Varian Cary Eclipse spectrofluorometer. Emission and excitation spectra were obtained with 10 nm excitation and 10 nm emission slit widths.

Luminescence quantum yields: Luminescence quantum yields were calculated from the average of three measurements relative to the reference value of $[Ru(bpy)_3]Cl_2$ (0.028 in air-saturated aqueous solution)[1] with the same absorbance at the wavelength of excitation (436 nm) for both samples, based on the equation (**1**):

$$\Phi_{em}^{\ i} = \frac{F^i A^{ref} \eta_i^2}{F^{ref} A^i \eta_{ref}^{\ 2}} \times \Phi_{em}^{ref} \qquad (\mathbf{1})$$

where *i* and *ref* refer to the sample and reference, respectively, Φ_{em} is the emission quantum yield, F is the integrated intensity of the luminescence spectrum, A is the absorbance at the excitation wavelength for the luminescence measurements and η is the solvent refractive index.

Time-resolved luminescence: Luminescence lifetimes were measured by single-photon timing (SPT) either on a Horiba Fluoromax-4TC-SPC or a Fluorolog FL 3-22 equipped with a FluoroHub v2.0 single-photon timing module using a sub-ns 405 nm pulsed diode laser (Horiba N-405L) or a 458 nm pulsed nanosecond light-emitting diode (Horiba N-460) as excitation source, respectively. The emission lifetimes were the average values obtained from a minimum of three replicate decay measurements with 10,000 counts at the peak channel. The decays were analysed using the Horiba DAS6 software, and the data were fitted to a sum of the minimum number of exponentials (n, equation (**2**)), employing the manufacturer proprietary grid-search error minimization algorithm,

$$I_{em}(t) = \sum_{i=1}^{n} a_i exp\left(-\frac{t}{\tau_i}\right) \qquad (\mathbf{2})$$

where $I_{em}(t)$ is the luminescence intensity at time t, a_i is the i^{th} pre-exponential factor and τ_i is the i^{th} emission lifetime.

For multi-exponential decays, the contribution of each component to the initial emission intensity (% A_i) was calculated according to equation (**3**):

$$\%A_i = \left[\frac{a_i\tau_i}{\sum_{i=1}^{n} a_i\tau_i}\right] \times 100 \quad (3)$$

The pre-exponential weighted mean lifetime, τ_M is given by equation (**4**):[2]

$$\tau_M = \sum_{i=1}^{n} \frac{a_i}{\sum_{i=1}^{n} a_i}\tau_i \quad (4)$$

The goodness-of-the-fit was assessed by the chi-squared value (always better than 1.1) as well as the symmetric distribution of the weighted residuals about the zero axis.

Synthesis and Characterisation

Ligands 1,4,5,8-tetraazaphenanthrene (TAP) and 5-amino-1,10-phenanthroline,[3] and the precursors complexes *cis*-[Ru(phen)$_2$Cl$_2$] and *cis*-[Ru(TAP)$_2$Cl$_2$],[4] were synthesised according to procedures previously reported in the literature.

***N*-1,10-phenanthrolin-5-yldocosamide (3):** 5-Amino-1,10-phenanthroline (101 mg, 515 µmol, 1 eq.) was dissolved in dry CH_2Cl_2 (10 mL) before the solution was cooled to 0 °C. Docosanoic acid (179 mg, 525 µmol, 1 eq.) was added to the solution followed by *N*-ethyl-*N*′-(3-dimethylaminopropyl)carbodiimide hydrochloride (255 mg, 1.33 mmol, 2.5 eq.) and, finally, 4-dimethylaminopyridine (65.0 mg, 532 µmol, 1 eq.). The resulting mixture was stirred under inert atmosphere and at 0 °C for 1 h before being allowed to reach room temperature and stirred for a further 2 days. Solvent was removed under reduced pressure and the resulting orange oil was dried *in vacuo*. H_2O was added causing precipitation of a beige solid which was isolated by centrifugation and washed several times with more H_2O. The resulting solid was redispersed in MeCN, collected by centrifugation and dried *in vacuo*, yielding the product as a beige solid (258 mg, 498 µmol, 95%). m.p. 90–93 °C. δ_H (600 MHz, $CDCl_3$): 9.18 (1H, d, H_2), 9.12 (1H, d, H_9), 8.31 (1H, d, H_4, ^3J = 8.4 Hz), 8.27 (1H, s, H_6), 8.21 (1H, dd, H_7 , ^3J = 8.1 Hz, ^4J = 1.2 Hz), 7.76 (1H, s, NH), 7.64 (1H, 2dd, H_3 and H_8, ^3J = 4.2 Hz, ^3J = 8.4 Hz, ^3J = 4.3 Hz, ^3J = 8.1 Hz), 2.58 (2H, m, $H_{2'}$), 1.84 (2H, m, $H_{3'}$), 1.36 (36H, m, $H_{4'}$–$H_{21'}$), 0.87 (3H, t, $H_{22'}$, ^3J = 6.8 Hz). δ_C (151 MHz, $CDCl_3$): 172.56 (C=O), 150.31, 149.93, 146.55 (q), 144.42 (q), 136.22, 130.67 (q), 129.84,

128.53 (q), 124.25 (q), 123.68, 122.97, 120.00, 37.82, 32.07, 29.85, 29.82, 29.81, 29.79, 29.67, 29.56, 29.51, 25.91, 22.84. ν_{max} (*ATR*)/cm^{-1}: 3262 (amide N-H stretch), 3046 (aromatic C-H stretch), 2915 and 2849 (alkane C-H stretch), 1657 (C=O stretch), 1541 (amide N-H bend), 1470 (aromatic C=C stretch), 1422 (C-N stretch). ESI$^+$-HRMS: m/z $_{calc}$ = 540.3924 for $C_{34}H_{51}N_3NaO$; m/z $_{found}$ = 540.3915 $[M+Na]^+$.

Bis(1,10-phenanthroline)(*N*-1,10-phenanthrolin-5-yldocosamide)ruthenium(II) chloride (1): The precursor complex *cis*-$[Ru(phen)_2Cl_2]$ (102 mg, 192 µmol, 1 eq.) and ligand **3** (145 mg, 281 µmol, 1.5 eq.) were suspended in a EtOH/H_2O mixture (1:1, 8 mL). The mixture was deoxygenated by sparging with argon for 15 min and the synthesis was carried out at 140 °C for 40 min under microwave irradiation. Solvent was evaporated at reduced pressure and the resulting solid was purified by alumina chromatography using MeCN/H_2O (10:0 to 9:1) as eluent, yielding the product as a red solid (101 mg, 96.0 µmol, 50%). Calculated for $C_{58}H_{67}N_7Cl_2ORu + 2.7H_2O + 0.1NaCl$: C, 63.06; H, 6.61; N, 8.88; Cl, 6.74. Found: C, 63.00; H, 6.08; N, 8.88; Cl, 6.70. m.p. 248–251 °C (decomp.). δ_H (600 MHz, DMSO-d_6): 10.51 (1H, s, NH), 8.93 (1H, dd, H_4^{L3}, ^3J = 8.6 Hz, ^4J = 1.0 Hz), 8.77 (4H, m, H^{phen}), 8.71 (1H, dd, H_7^{L3}, ^3J = 8.3 Hz, ^4J = 0.8 Hz), 8.66 (1H, s, H_6^{L3}), 8.39 (4H, s, H_5^{phen} and H_6^{phen}), 8.08 (4H, m, H^{phen}), 8.05 (1H, dd, H_2^{L3}, ^3J = 5.2 Hz, ^4J = 1.0 Hz), 7.96 (1H, dd, H_9^{L3}, ^3J = 5.2 Hz, ^4J = 0.8 Hz), 7.77 (5H, m, H_3^{L3} and H^{phen}), 7.69 (1H, dd, H_8^{L3}, ^3J = 8.3 Hz, ^3J = 5.2 Hz), 2.60 (2H, t, $H_{2'}^{L3}$, ^3J = 7.4 Hz), 1.69 (2H, m, $H_{3'}^{L3}$), 1.29 (36H, m, $H_{4'}$–$H_{21'}^{L3}$), 0.84 (3H, t, $H_{22'}^{L3}$, ^3J = 7.0 Hz). δ_C (151 MHz, DMSO-d_6): 172.79 (C=O), 152.74, 151.51, 147.59 (q), 147.22 (q), 147.20 (q), 147.18 (q), 144.82 (q), 136.83, 136.19, 133.87 (q), 132.64, 130.44 (q), 130.23 (q), 128.04, 126.35, 126.28, 125.53 (q), 119.07, 36.05, 31.27, 29.00, 28.97, 28.94, 28.82, 28.68, 25.19, 22.07, 13.94. ν_{max} (*ATR*)/cm^{-1}: 3185 (amide N-H stretch), 3044 (aromatic C-H stretch), 2920 and 2848 (alkane C-H stretch), 1698 (C=O stretch), 1541 (amide N-H bend), 1458 (aromatic C=C stretch), 1424 (C-N stretch). ESI$^+$-HRMS: m/z $_{calc}$ = 979.4451 for $C_{58}H_{67}N_7ORu$; m/z $_{found}$ = 489.7232 $[M]^{2+}$.

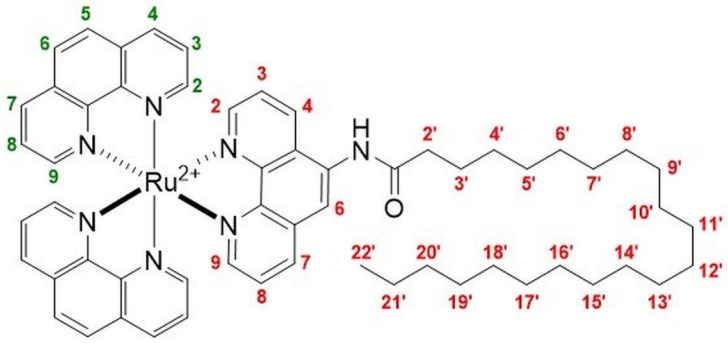

Bis(1,4,5,8-tetraazaphenanthrene)(*N*-1,10-phenanthrolin-5-yldocosamide)ruthenium(II) chloride (2): Complex **2** was synthesised according to the same procedure described for **1** but using the precursor complex *cis*-$[Ru(TAP)_2Cl_2]$ (103 mg, 192 µmol, 1 eq.) and ligand **3** (122 mg, 236 µmol, 1.2 eq.), and yielding the product as a red solid (84.4 mg, 80.0 µmol, 42%). Calculated for $C_{54}H_{63}N_{11}Cl_2ORu$ + $4.7H_2O$ + 0.1NaCl: C, 56.66; H, 6.38; N, 13.46; Cl, 6.50. Found: C, 56.50; H, 5.82; N, 13.45; Cl, 6.38. m.p. 171–172 °C (decomp.). δ_H (400 MHz, CD_3CN): 11.63 (1H, s, NH), 9.71 (1H, dd, H_4^{L3}, ^3J = 8.6 Hz, ^4J = 1.1 Hz), 8.93 (4H, m, H^{TAP}), 8.70 (1H, s, H_6^{L3}), 8.60 (5H, m, H_7^{L3}, H_9^{TAP} and H_{10}^{TAP}), 8.27 (1H, d, H^{TAP}, ^3J = 2.8 Hz), 8.26 (1H, d, H^{TAP}, ^3J = 2.8 Hz), 8.19 (1H, d, H^{TAP}, ^3J = 2.8 Hz), 8.14 (2H, m, H^{TAP} and H_2^{L3}), 7.99 (1H, dd, H_9^{L3}, ^3J = 5.2 Hz, ^4J = 1.2 Hz), 7.71 (1H, dd, H_3^{L3}, ^3J = 5.2 Hz, ^3J = 8.6 Hz), 7.60 (1H, dd, H_8^{L3}, ^3J = 5.2 Hz, ^3J = 8.3 Hz), 2.84 (2H, t, $H_{2'}^{L3}$, ^3J = 7.4 Hz), 1.75 (2H, m, $H_{3'}^{L3}$), 1.32 (36H, m, $H_{4'}$–$H_{21'}^{L3}$), 0.87 (3H, t, $H_{22'}^{L3}$, ^3J = 7.0 Hz). δ_C (101 MHz, CD_3CN): 174.97 (C=O), 154.70, 153.20, 150.36, 150.32, 150.30, 150.08, 150.04, 149.79, 149.64, 146.37 (q), 146.34 (q), 146.32 (q), 145.37 (q), 143.33 (q), 143.27 (q), 138.39, 136.86, 136.19 (q), 133.75, 133.58, 132.14 (q), 128.31 (q), 126.93, 126.03, 119.95, 37.34, 32.56, 30.31, 30.29, 30.18, 29.99, 26.53, 23.32, 14.32. ν_{max} (*ATR*)/cm^{-1}: 3245 (amide N-H stretch), 3050 (aromatic C-H stretch), 2920 and 2851 (alkane C-H stretch), 1686 (C=O stretch), 1535 (amide N-H bend), 1485 (aromatic C=C stretch), 1423 (C-N stretch), 1384 (C-N stretch). MALDI$^+$-HRMS: m/z_{calc} = 983.4261 for $C_{54}H_{63}N_{11}ORu$; m/z_{found} = 983.4290 $[M]^+$.

Singlet Oxygen Photosensitisation

Direct detection of singlet oxygen (time-resolved near infrared phosphorescence): Quantum yields of singlet oxygen production were measured using an Edinburgh Instruments (UK) LP-900 laser kinetic spectrometer system equipped with a frequency-doubled Nd:YAG laser (Minilite II, Continuum, CA) for excitation at 532 nm, and a Hamamatsu H10330-45 NIR PMT module for the singlet oxygen emission monitoring at 1265 nm (Bentham TM300 monochromator with 600 grooves mm^{-1} NIR grating). The PMT is fitted with a 10 KΩ resistor at the signal output for proper

amplification of the signal. A pyroelectric Gentec QE12LP-S-MB energy meter was employed to monitor the energy of the laser pulse, which was varied from 100 to 1000 μJ pulse^{-1} to avoid partial saturation of the $^1O_2$ emission signal and to keep it in the linear region.

Absorbance-matched ($A_{532} \approx 0.40$) solutions of the ruthenium complex and the reference photosensitiser $[Ru(phen)_3]Cl_2$ ($\Phi_\Delta = 0.39 \pm 0.03$ in O_2-saturated D_2O at room temperature)[6] were prepared in D_2O. The solutions were then saturated by sparging with O_2 from a cylinder (Extrapure oxygen 4X, Praxair, ES) for a minimum of 30 min. The NIR emission from the sample was monitored at a 90° angle with respect to the excitation pathway and detected with the NIR PMT after passing through an interference filter centred at 1265 nm (77-nm FWMH, Roithner-laser, AT). Typically, 60 laser shots were averaged for each signal to improve the s/n ratio.

The $^1O_2$ luminescence decay profiles were fitted to a single exponential function after excluding the fast (sub-μs) decay due to the residual Ru(II) sensitiser emission even under O_2 saturation of the solution. The quality of the D_2O solvent used was checked by measuring the $^1O_2$ luminescence lifetime of the sensitiser solutions (*ca.* 65 μs).[6,7] After extrapolating the intensities of the $^1O_2$ signal at zero time within each exponential decay curve, the intercept values were plotted as a function of the laser energy. The slope values (m) obtained from the linear regression plots of the sample and reference sensitiser dyes were used to calculate the quantum yields of singlet oxygen production (Φ_Δ) for the different Ru(II) complexes in O_2-saturated D_2O according to equation (**6**):

$$\Phi_{\Delta,\,D_2O,\,O_2}^{complex} = \Phi_{\Delta,\,D_2O,\,O_2}^{ref} \frac{m_{complex}}{m_{ref}} \qquad (\mathbf{6})$$

From the experimental data obtained in D_2O, the Φ_Δ values in air-equilibrated H_2O were calculated taking into account equations (**7**) and (**8**):[8]

$$P_{O_2}^T = \tau k_q [O_2] = 1 - \frac{\tau}{\tau_0} \qquad (\mathbf{7})$$

$$\Phi_\Delta = \Phi_T P_{O_2}^T f_\Delta^T \qquad (\mathbf{8})$$

where $P_{O_2}^T$ is the fraction of triplet excited states of the photosensitiser quenched by O_2, k_q is the O_2 quenching rate constant, τ and τ_0 are the emission lifetimes in the presence and in the absence

of O_2, respectively, Φ_T is the quantum yield of triplet excited-state formation (intersystem crossing), and f_{Δ}^{T} is the fraction of excited triplet states quenched by O_2 to yield $^1O_2$.

Knowing that Φ_T is considered to be equal to 1 for this type of complexes,[8] and assuming that f_{Δ}^{T} is the same in O_2-saturated D_2O and air-saturated H_2O, Φ_{Δ} values in air-equilibrated H_2O were calculated according to equation (**9**):

$$\Phi_{\Delta,H_2O,\,air}^{complex} = \Phi_{\Delta,D_2O,\,O_2}^{complex}\left(1-\frac{\tau_{H_2O,\,air}}{\tau_{H_2O,\,Ar}}\right)\Big/\left(1-\frac{\tau_{D_2O,\,O_2}}{\tau_{D_2O,\,Ar}}\right) \qquad (\mathbf{9})$$

Indirect detection of singlet oxygen (photo-oxidation of a chemical probe): Singlet oxygen production was also evaluated using the water soluble $^1O_2$ trap 9,10-anthracenediyl-bis(methylene)dimalonic acid (ABDA).[9] Aqueous solutions containing the Ru(II) complex (A_{470} ≈ 0.01) and ABDA (2 μM, stock solution in 10 mM sodium phosphate-buffered aqueous solution) were irradiated in a 1 × 1 cm Spectrosil cuvette under continuous stirring using a CoolLED pE-2 microscope LED illumination source (470 nm, 100% intensity). The disappearance of the fluorescence of ABDA at 405 nm (λ_{exc} = 380 nm) was monitored at different irradiation times. The UV-vis absorption spectra of the solutions containing the Ru(II) complex and ABDA were also recorded before and after irradiation to show that the Ru(II) were stable under the photolysis conditions (Fig. S18). In order to exclude any degradation of ABDA upon irradiation, the emission spectrum of ABDA in the absence of Ru(II) complex was also recorded at different irradiation times (Fig. S19).

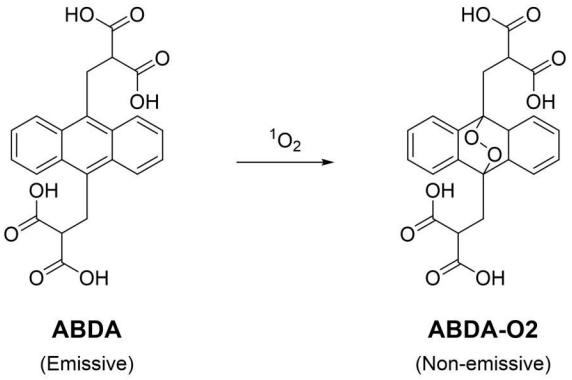

ABDA (Emissive) **ABDA-O2** (Non-emissive)

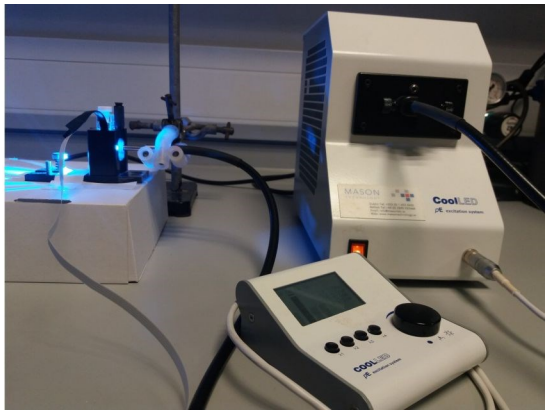

Surface Tension Measurements

Surface tension was measured with a Kibron EZ-PI Plus Surface Tensiometer for automatic measurement of surface and interfacial tension fitted with a 0.5 mm diameter metallic rod (Kibron DyneProbe) and a polypropene sample cup. Individual aqueous solutions (3 mL) at different surfactant concentrations were prepared and left to equilibrate for 16 h before surface tension was measured at 20 °C.

Partition Coefficients (log *P*)

Partition coefficients were determined by the "shake-flask" method.[5] The appropriate Ru(II) complex was dissolved in 1 mL of water (pre-saturated with 1-octanol) and the concentration was determined by UV-vis absorption spectroscopy. An equivalent volume of 1-octanol (pre-saturated with water) was added and both phases were shaken for 1 h. The mixture was centrifuged for 1 h at 3000 rpm in order to separate the phases and then equilibrated for a further 16 h. The concentration of the complex in the aqueous phase was determined by UV-vis absorption spectroscopy. The log *P* values were calculated according to equation (**5**):

$$log\ P = log\left(\frac{c_t - c_{water}}{c_{water}}\right) \quad \textbf{(5)}$$

where c_t is the total concentration of complex in the aqueous phase before adding 1-octanol and c_{water} is the concentration of complex in the aqueous phase after adding 1-octanol and shaking.

Cellular Uptake Studies

HeLa cells were seeded at a density of 5×10^4 cells/mL and treated as indicated. Cells were then washed twice with fresh medium and stained blue with Hoechst 33258 (10 μg/mL) when appropriate before being imaged by live microscopy using an Olympus FV1000 point scanning microscope with a 60x oil immersion lens (NA 1.42). A 405 nm diode laser was used to excite both the Hoechst dye and the appropriate Ru(II) complex and the emission was measured at 415–505 nm and 610–715 nm, respectively. The software used to collect images was FluoView Version 7.1 software.

Viability Assays

HeLa cells were seeded at a density of 2.5×10^3 cells/mL in a 96-well plate and treated with different concentrations of the appropriate Ru(II) complex. Into each well was then added 20 μL

of Alamar Blue (BioSource) and left incubating at 37 °C in the dark for 4 h. Fluorescence was read using a fluorescence microplate reader (SpectraMax Gemini XS, Molecular Devices) at 590 nm (excitation at 544 nm). The data were analysed using the SoftMax® Pro Software. The background fluorescence of the media without cells plus Alamar Blue was taken away from each group, and the control untreated cells represented 100% cell viability. Data points represent the mean ± S.E.M. of triplicate treatments performed on three independent days with activity expressed as percentage cell viability compared to vehicle treated controls. For photoactivation studies, cells were subjected to 18 J cm^{-2} using a Hamamatsu L2570 200 W Hg-Xe arc lamp equipped with a $NaNO_2$ filter.

Intracellular ROS Generation

HeLa cells were incubated with the appropriate Ru(II) complex (5 μM) at 37 °C for 30 min before the ROS indicator 2',7'-dichlorodihydrofluorescein diacetate (DCFH-DA, 20 μM) was added. A control experiment in the absence of ruthenium complex was also performed (Fig. S20). After a further 30 min incubation, cells were washed twice with fresh medium and irradiated using a 405 nm diode laser attached to a Leica SP8 gated STED confocal microscope with a 40x oil immersion lens (NA 1.30). Images were taken every 1.3 s over a 3 min period time. A 470–670 supercontinuum laser ("White Light Laser"), from which the 498 nm radiation was selected, was used to excite the DCFH-DA and fluorescence was measured at 510–570 nm. The software used to collect images was Leica Application Suite X (LAS X).

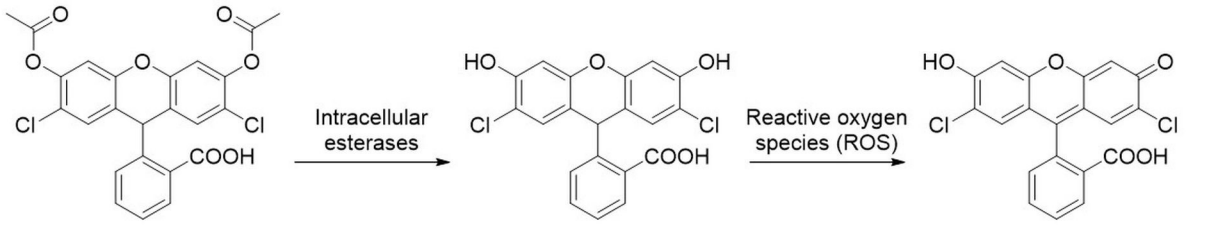

References:

1. A. M. Brouwer, *Pure Appl. Chem.*, 2011, **83**, 2213.
2. E. R. Carraway, J. N. Demas and B. A. DeGraff, *Anal. Chem.*, 1991, **63**, 332.

3. R. Nasielski-Hinkens, M. Benedek-Vamos, Y. Hautain and J. Nasielski, *Bull. Soc. Chim. Belg.*, 1976, **85**, 781; J. P. Lecomte, A. Kirsch-De Mesmaeker, M. Demeunynck and J. Lhomme, *J. Chem. Soc., Faraday Trans.*, 1993, **89**, 3261.
4. T. Doi, H. Nagamiya, M. Kokubo, K. Hirabayashi and T. Takahashi, *Tetrahedron*, 2002, **58**, 2957.
5. J. Sangster, *Octanol-Water Partition Coefficients: Fundamentals and Physical Chemistry*, Wiley, 1997.
6. A. Hergueta-Bravo, M. E. Jiménez-Hernández, F. Montero, E. Oliveros and G. Orellana, *J. Phys. Chem. B*, 2002, **106**, 4010.
7. L. A. Martinez, C. G. Martínez, B. B. Klopotek, J. Lang, A. Neuner, A. M. Braun and E. Oliveros, *J. Photochem. Photobiol., B*, 2000, **58**, 94.
8. D. García-Fresnadillo, Y. Georgiadou, G. Orellana, A. M. Braun and E. Oliveros, *Helv. Chim. Acta*, 1996, **79**, 1222.
9. M. González-Béjar, M. Liras, L. Francés-Soriano, V. Voliani, V. Herranz-Pérez, M. Duran-Moreno, J. M. Garcia-Verdugo, E. I. Alarcon, J. C. Scaiano and J. Pérez-Prieto, *J. Mater. Chem. B*, 2014, **2**, 4554.

Supporting Figures and Tables

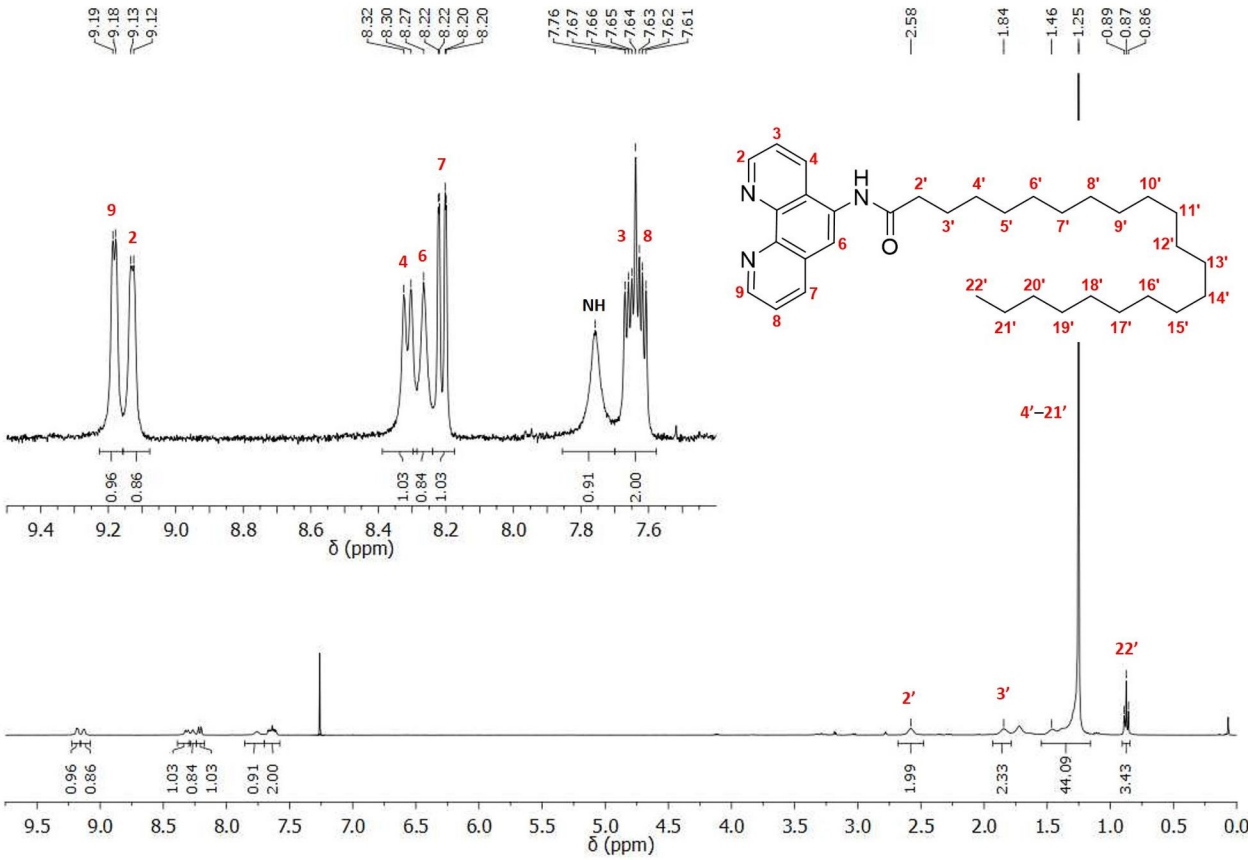

Fig. S1. ^{1}H NMR (600 MHz, $CDCl_3$) spectrum of ligand **3**.

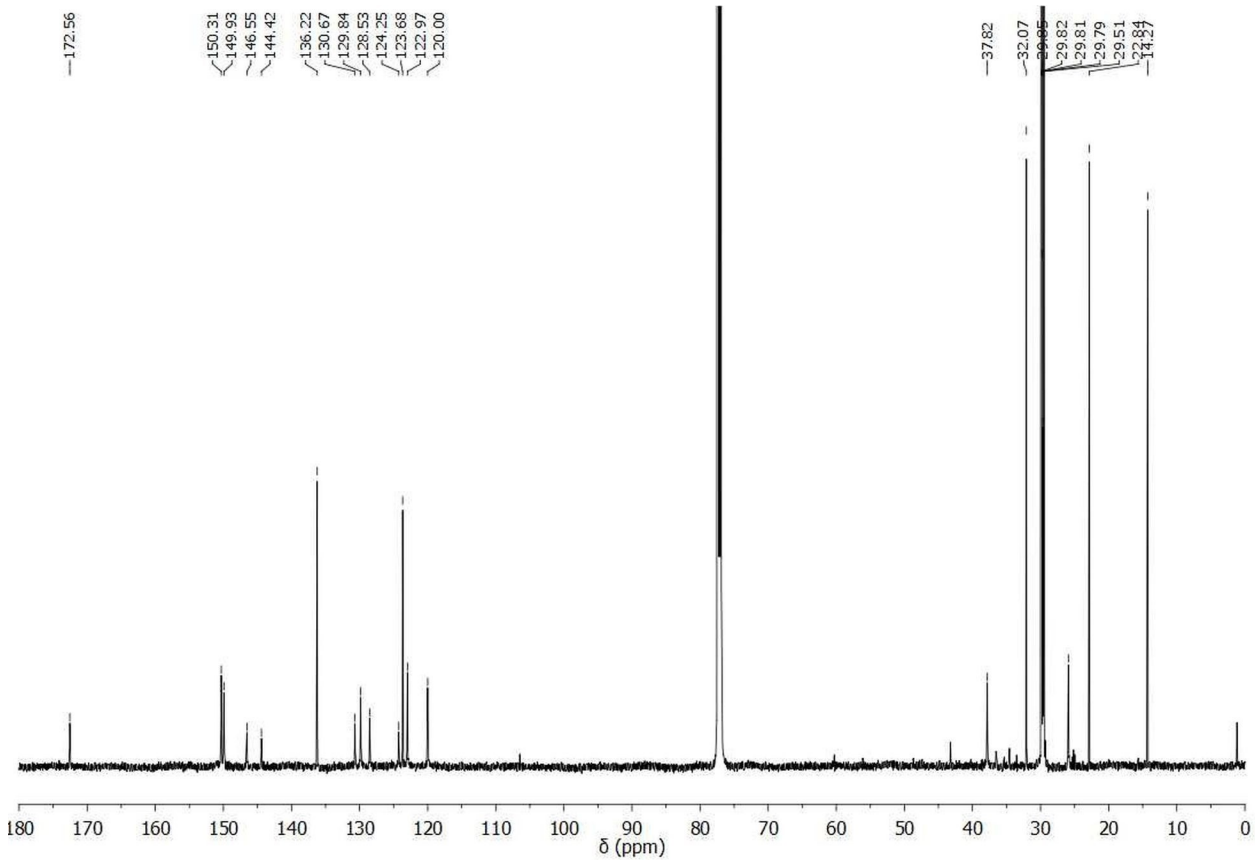

Fig. S2. ^{13}C NMR (151 MHz, $CDCl_3$) spectrum of ligand **3**.

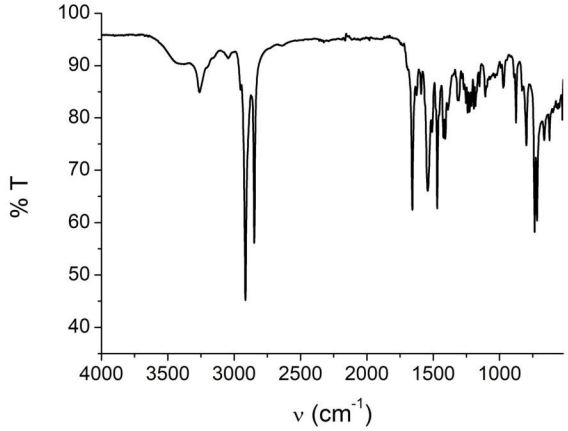

Fig. S3. FTIR spectrum of ligand **3**.

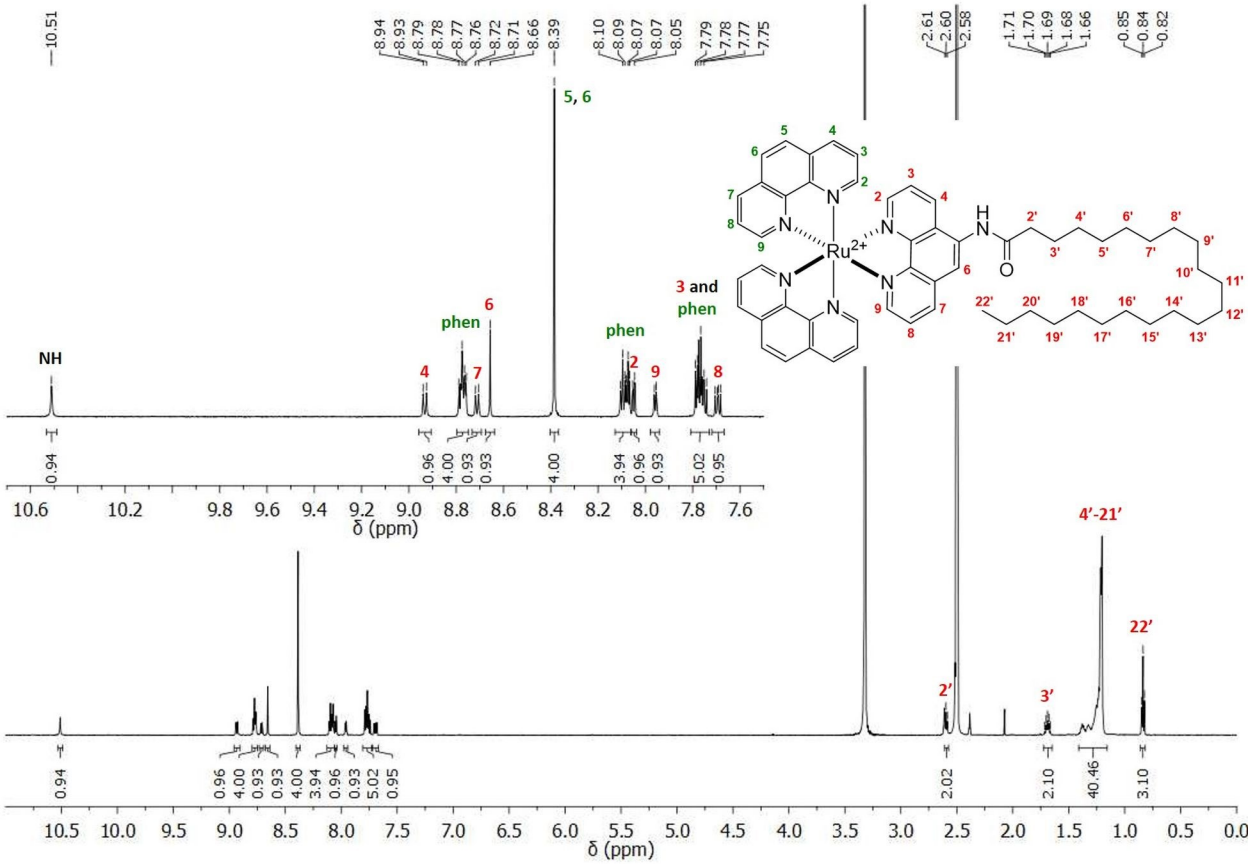

Fig. S4. ^{1}H NMR (600 MHz, DMSO-d_6) spectrum of complex **1**. Signals corresponding to **phen** ligands are in green and signals assigned to ligand **3** are in red.

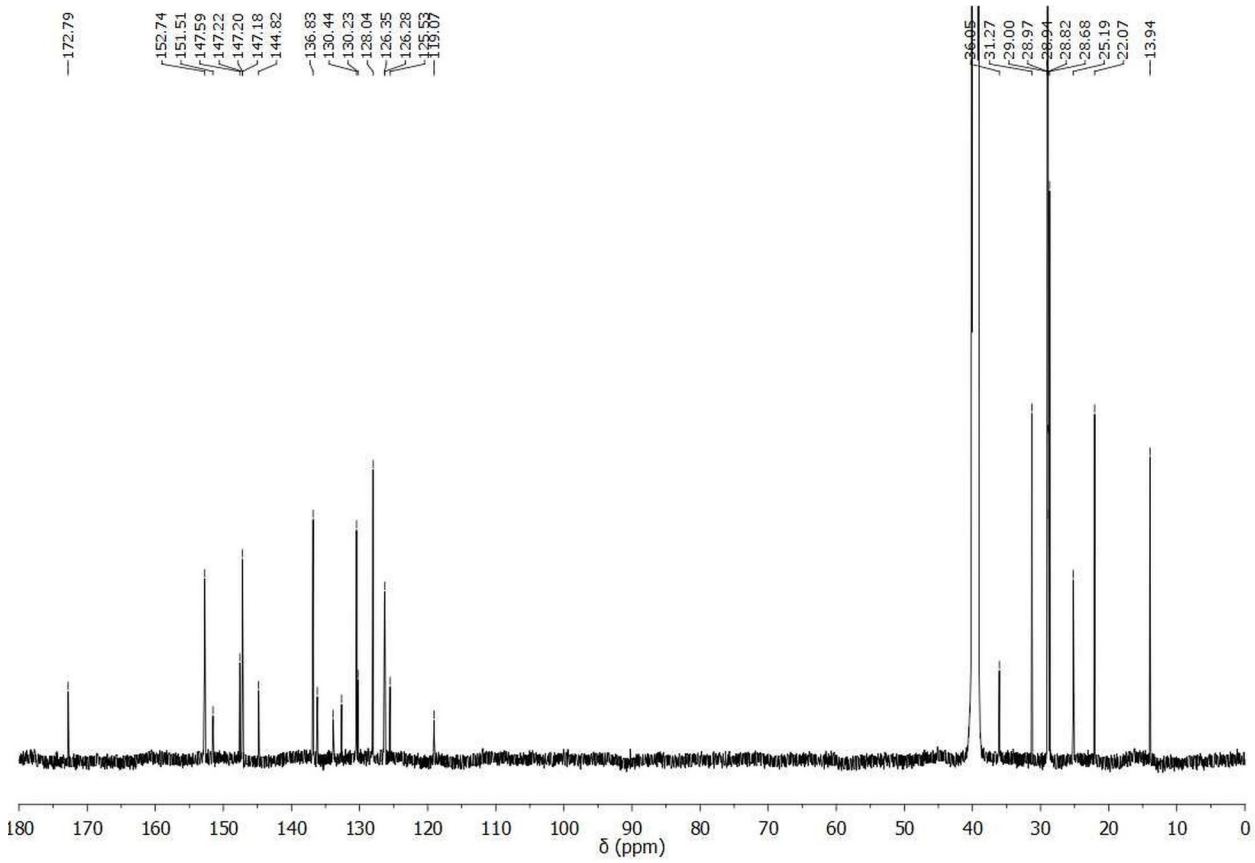

Fig. S5. ^{13}C NMR (151 MHz, DMSO-d_6) spectrum of complex **1**.

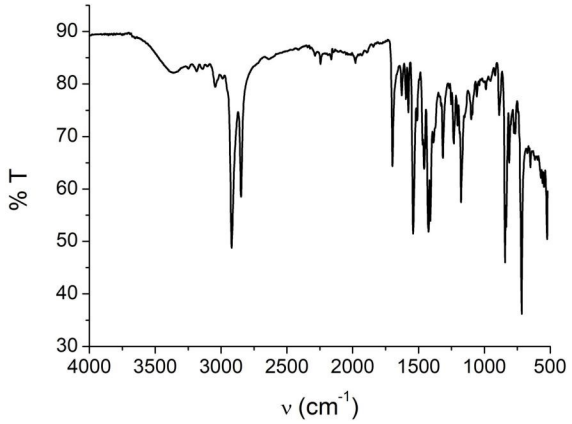

Fig. S6. FTIR spectrum of complex **1**.

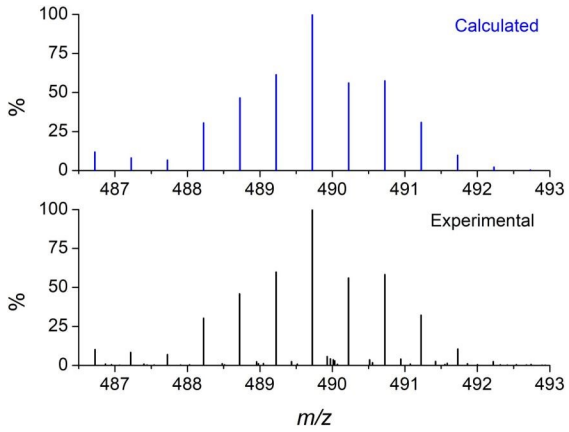

Fig. S7. Comparison between the calculated (blue) and experimental (black) isotopic distribution pattern for complex **1** from electrospray ionisation (positive mode) high resolution mass spectrometry analysis.

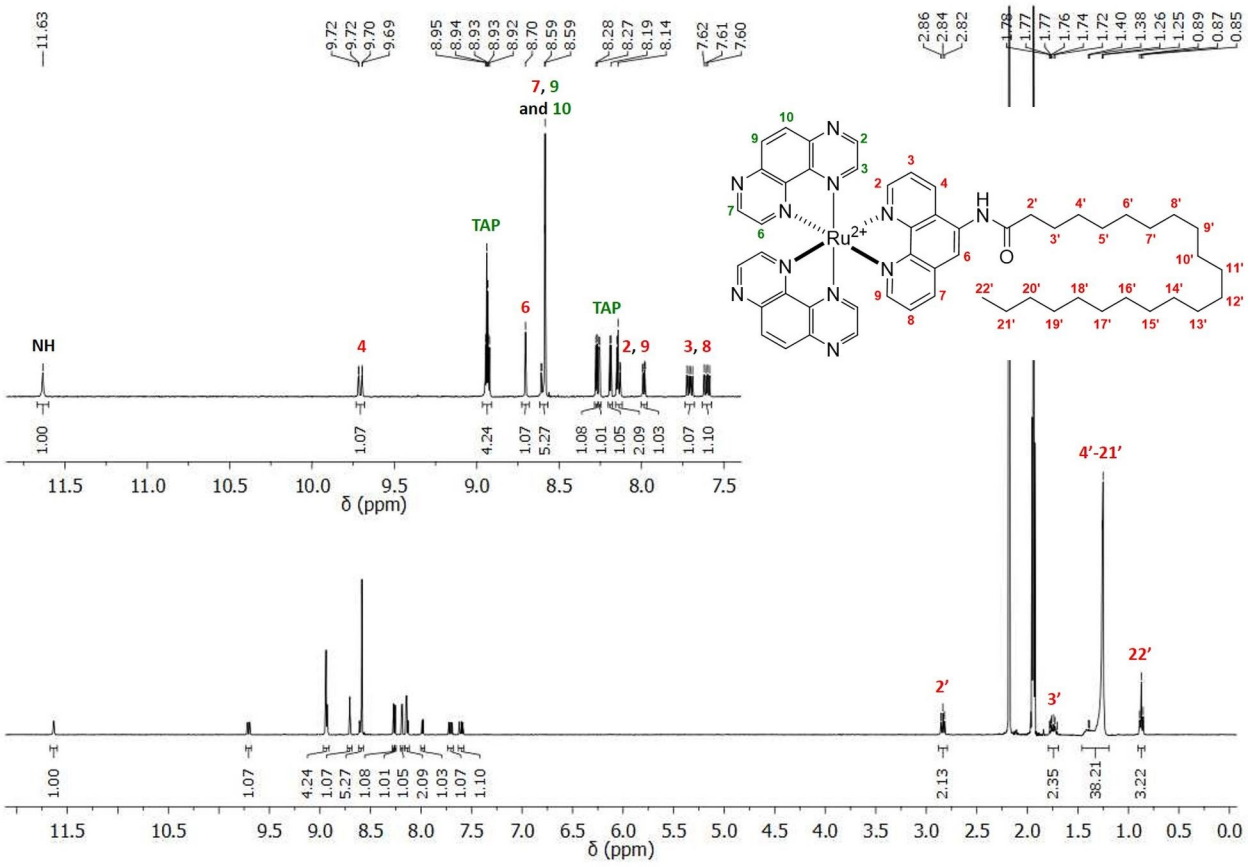

Fig. S8. ^{1}H NMR (400 MHz, CD_3CN) spectrum of complex **2**. Signals corresponding to **TAP** ligands are in green and signals assigned to ligand **3** are in red.

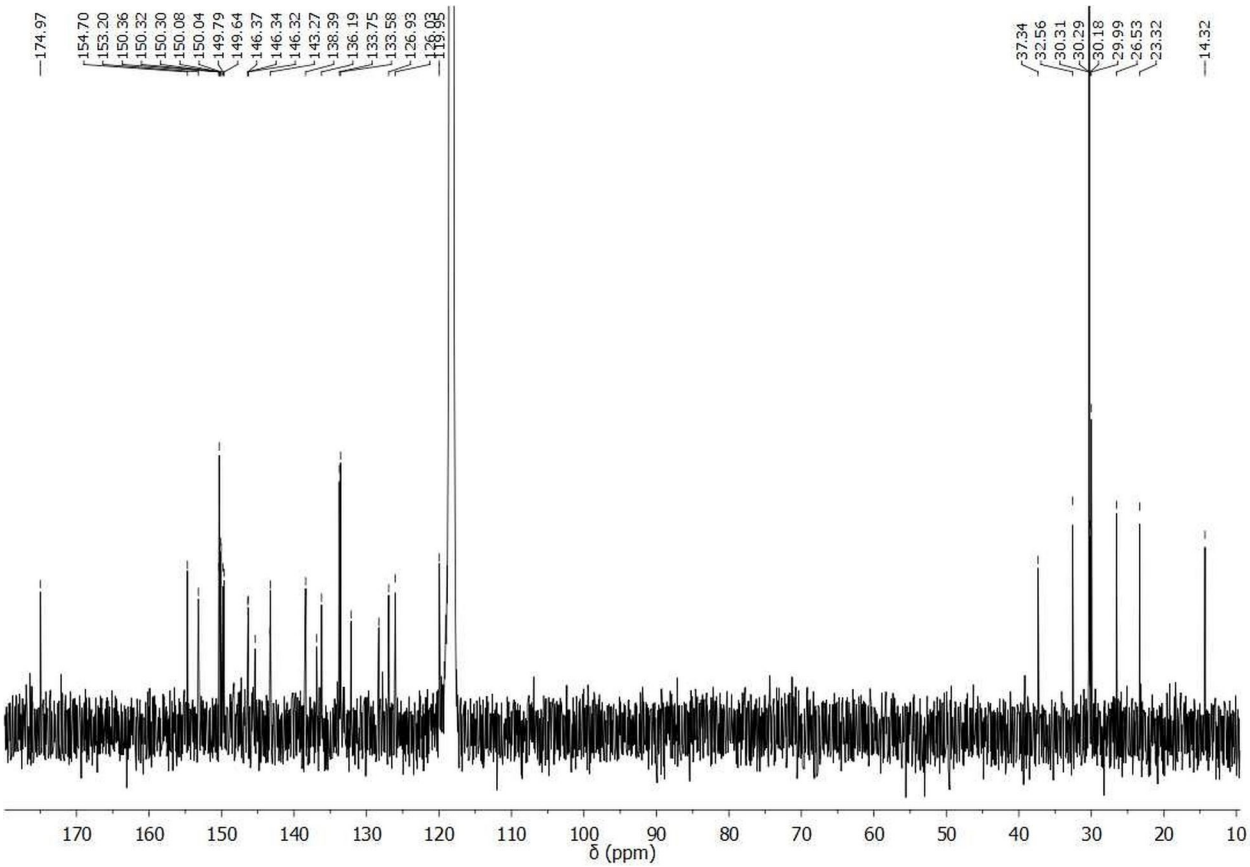

Fig. S9. ^{13}C NMR (101 MHz, CD_3CN) spectrum of complex **2**.

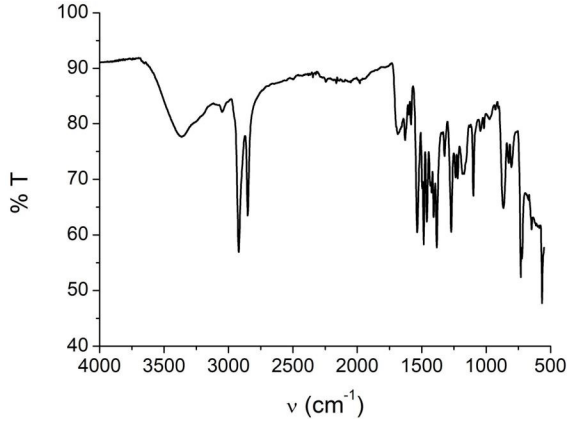

Fig. S10. FTIR spectrum of complex **2**.

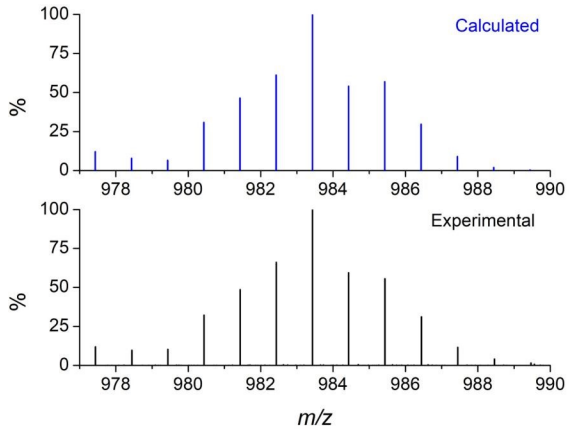

Fig. S11. Comparison between the calculated (blue) and experimental (black) isotopic distribution pattern for complex **2** from matrix-assisted laser desorption/ionisation (positive mode) high resolution mass spectrometry analysis.

Table S1. Bi-exponential and pre-exponential weighted mean emission lifetimes (τ_M) of **1** and **2** in aerated and deoxygenated (N_2) 10 mM sodium phosphate-buffered aqueous solution at pH 7.4, at 298 K.

Complex	Conditions	τ_1 (ns)	%A_1	τ_2 (ns)	%A_2	τ_M (ns)
1	Air	759	39	1490	61	1085
	N_2	896	31	1752	69	1354
2	Air	358	30	813	70	587
	N_2	343	20	949	80	696

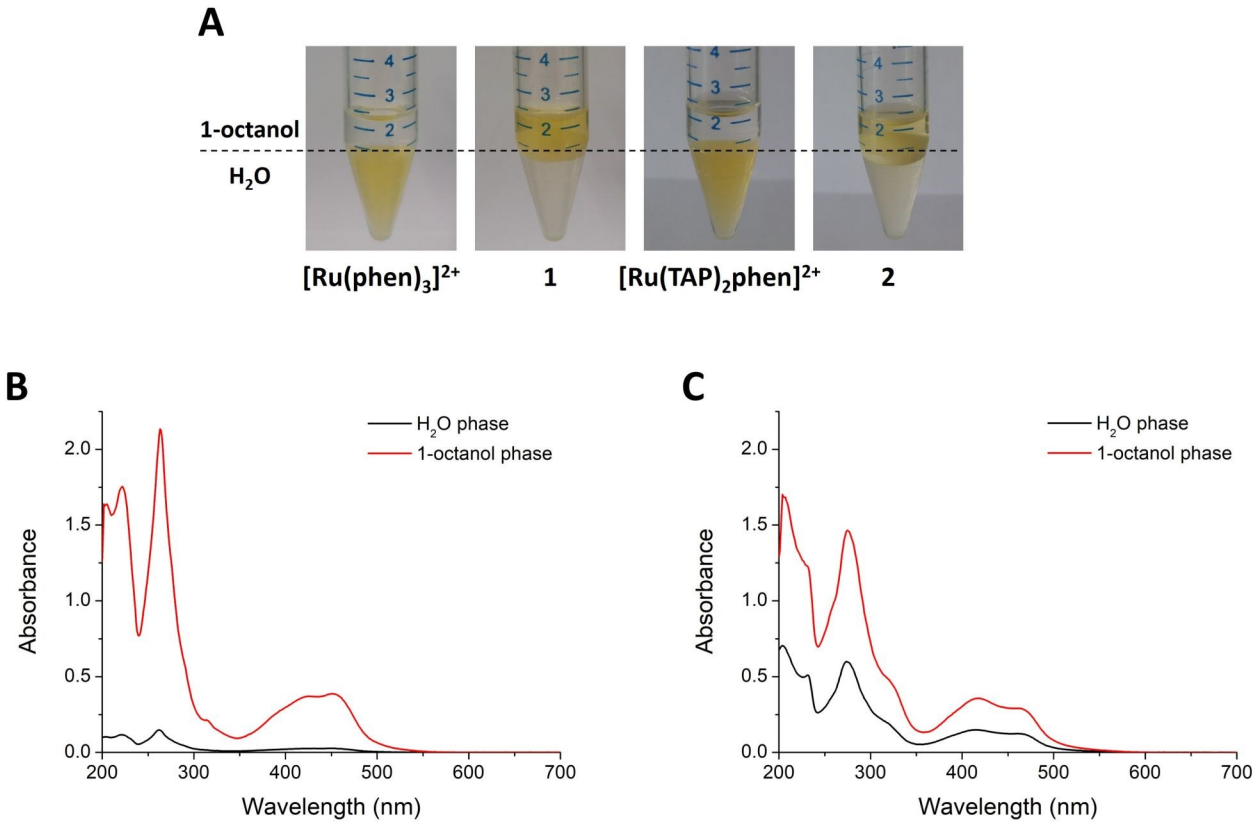

Fig. S12. (A) Partition studies of $[Ru(phen)_3]^{2+}$, **1**, $[Ru(TAP)_2phen]^{2+}$ and **2** (50 μM) between 1-octanol and water phases. UV-vis absorption spectra of (B) **1** and (C) **2** in water (black) and 1-octanol (red) phases at 298 K, showing the preference of both complexes by the 1-octanol phase.

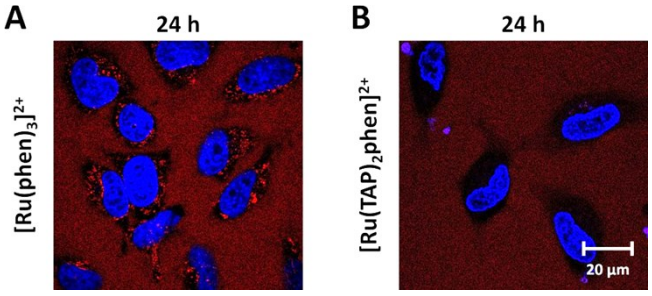

Fig. S13. Confocal fluorescence microscopy images showing HeLa cells do not take up (A) $[Ru(phen)_3]^{2+}$ and (B) $[Ru(TAP)_2phen]^{2+}$ (red, 50 μM) after 24 h incubation. The nucleus is stained blue with Hoechst 33258.

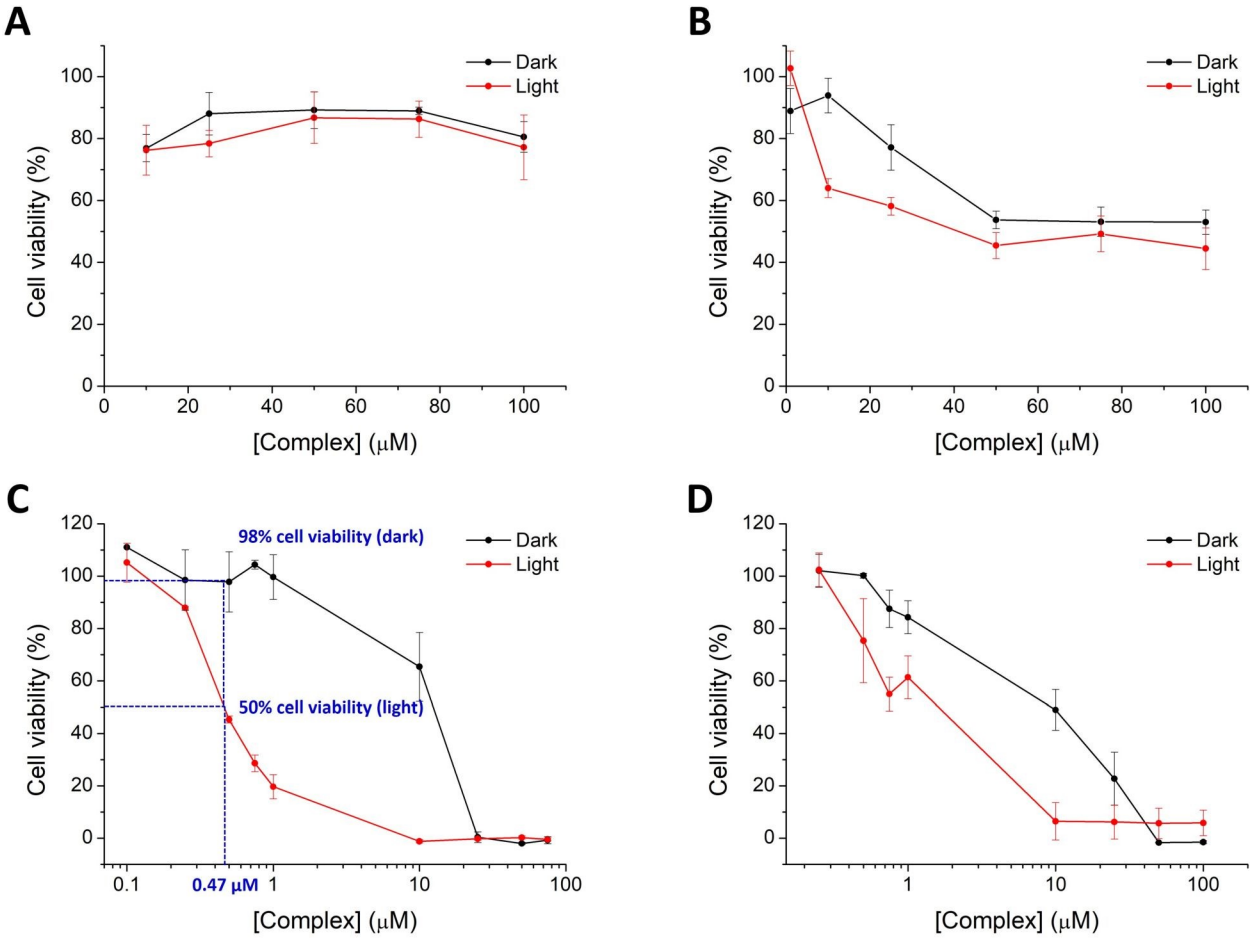

Fig. S14. Toxicity profiles of (A) $[Ru(phen)_3]^{2+}$, (B) $[Ru(TAP)_2phen]^{2+}$, (C) **1** and (D) **2** in HeLa cells. Note that a logarithmic scale is used in graphs (C) and (D) for the sake of clarity.

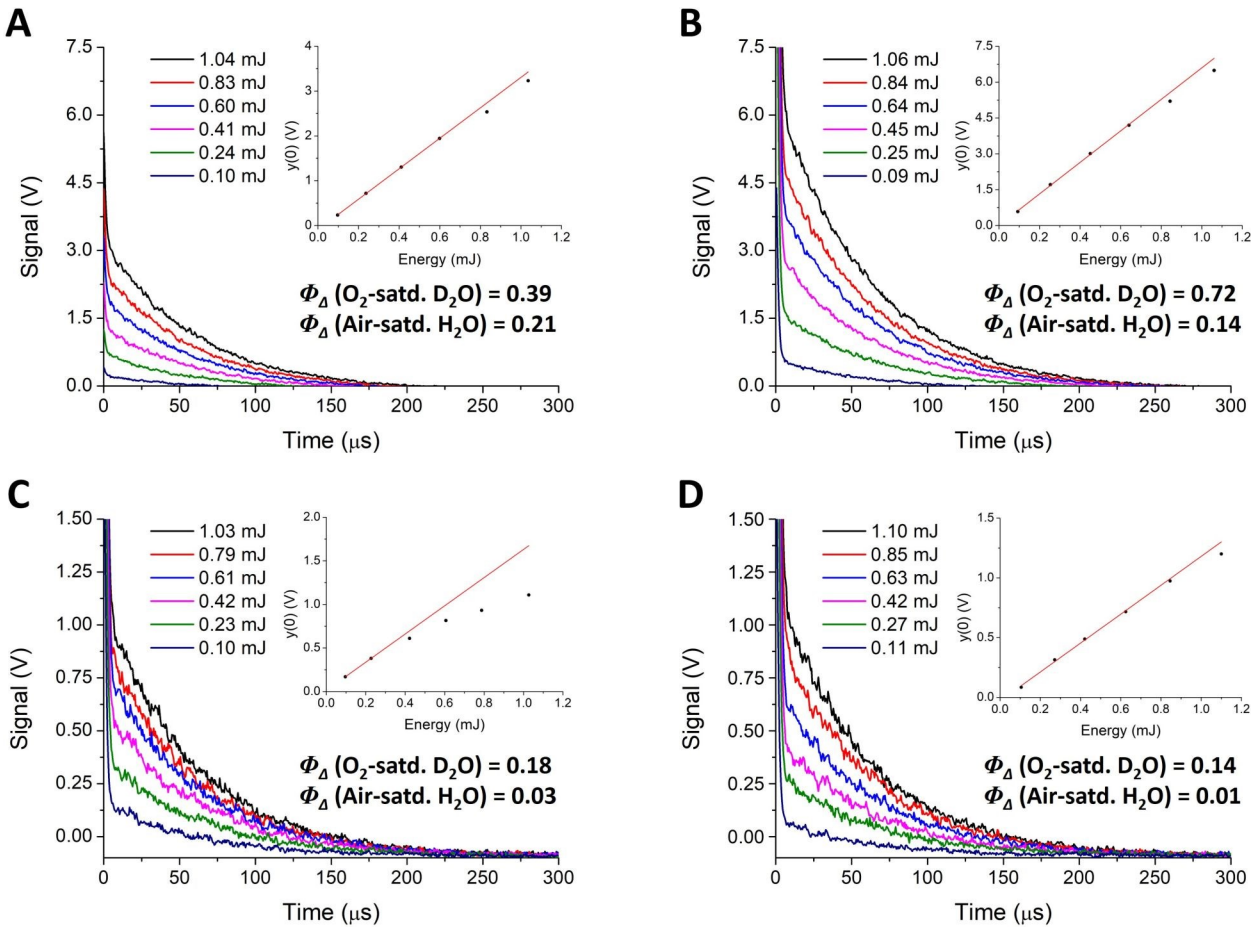

Fig. S15. Singlet oxygen emission decays at 1270 nm produced by (A) $[Ru(phen)_3]^{2+}$, (B) $[Ru(TAP)_2phen]^{2+}$, (C) **1** and (D) **2** at different laser energies (λ_{exc} = 532 nm) in O_2-saturated D_2O solution at 298 K. Inset: Plot of intercept values (V) *vs.* laser energy (mJ) and the best linear fit of the data.

Table S2. Emission lifetimes (τ_{em}) measured in O_2- and argon-saturated D_2O, and in air- and Ar-saturated H_2O, and quantum yields of singlet oxygen production (Φ_Δ) in O_2-saturated D_2O and air-saturated H_2O for $[Ru(phen)_3]^{2+}$, $[Ru(TAP)_2phen]^{2+}$, **1** and **2**.

Complex	τ_{em} (ns) (O_2, D_2O)[a]	τ_{em} (ns) (Ar, D_2O)[a]	τ_{em} (ns) (Air, H_2O)[a]	τ_{em} (ns) (Ar, H_2O)[a]	Φ_Δ (O_2-satd. H_2O)[b]	Φ_Δ (Air-satd. H_2O)
$[Ru(phen)_3]^{2+}$	180	1154	505	933	0.39	0.21
$[Ru(TAP)_2phen]^{2+}$	480	1724	724	840	0.72	0.14
1	361[c]	719[c]	876[c]	947[c]	0.18[d]	0.03
2	326[c]	985[c]	770[c]	825	0.14	0.01

[a] If not otherwise indicated, the luminescence decays are monoexponential. Estimated errors ±5%.
[b] O_2-saturated D_2O solution of $[Ru(phen)_3]Cl_2$ as reference (Φ_Δ = 0.39). Estimated errors ±5%.
[c] The luminescence decays are bi- or tri-exponential; reported data correspond to the pre-exponential weighted mean lifetimes.
[d] Calculated from the linear fit of the data at low laser energy due to deviation from linearity of the data at high laser energy.

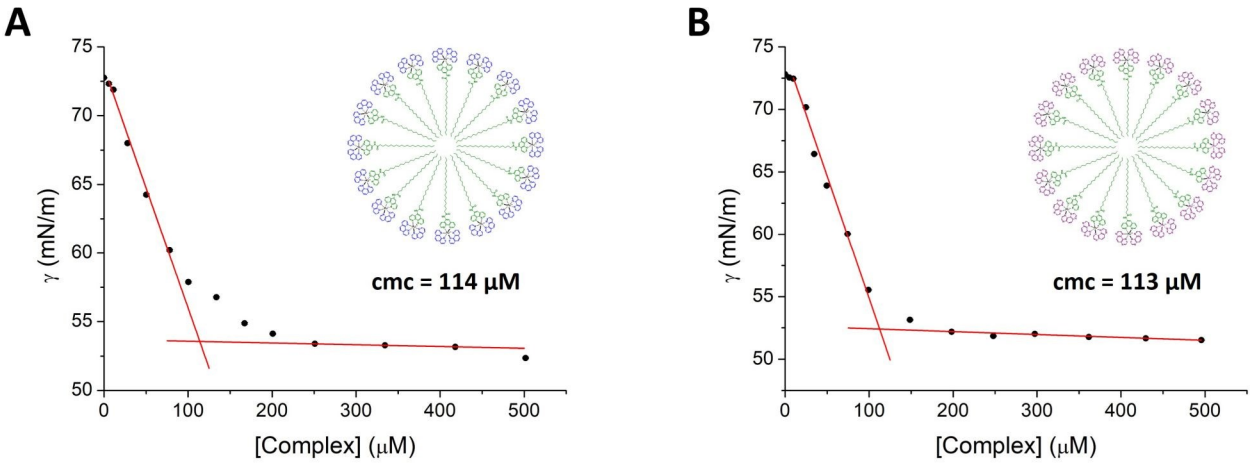

Fig. S16. Determination of the critical micelle concentration by surface tension measurements of aqueous solutions of (A) **1** and (B) **2** at different concentrations, at 293 K.

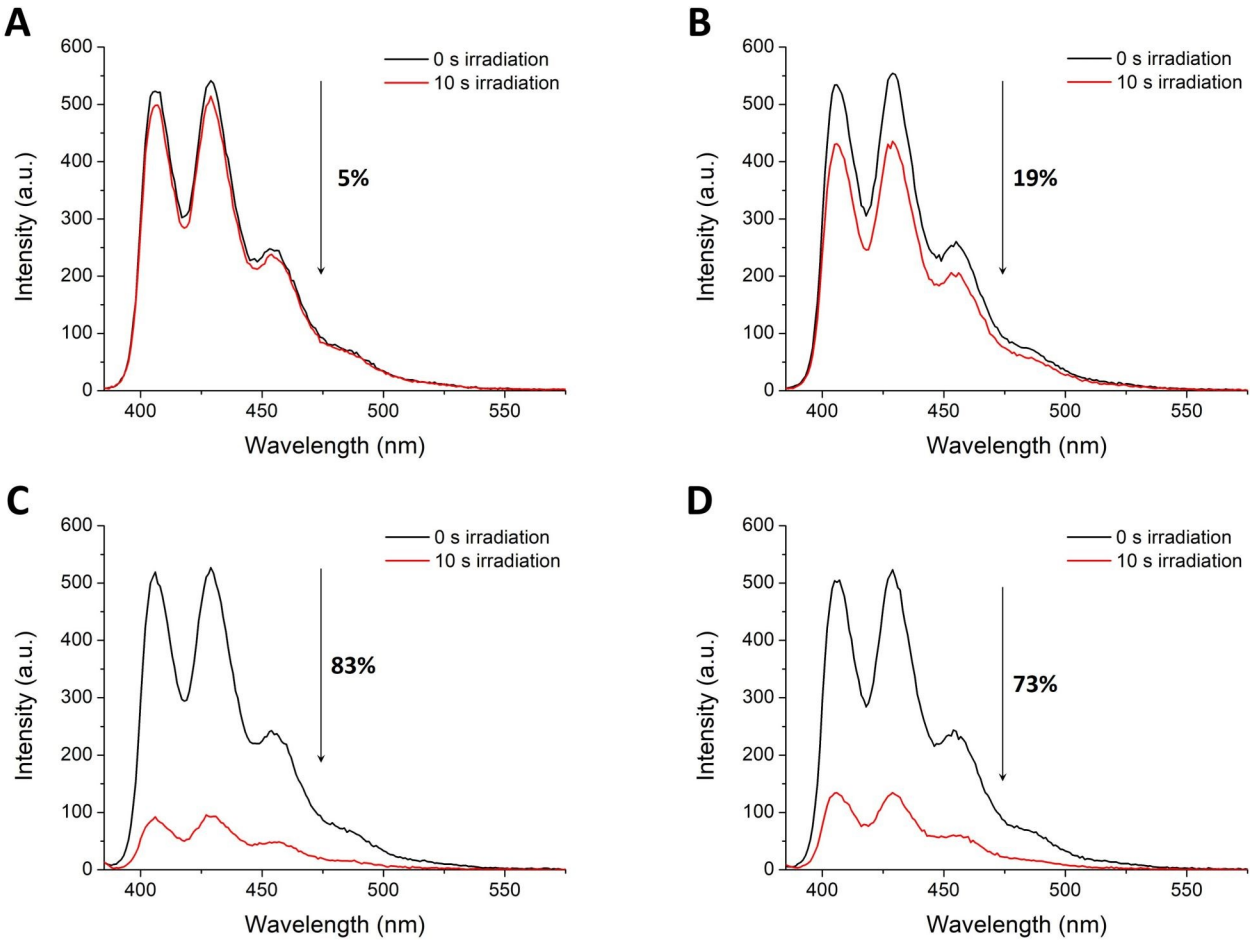

Fig. S17. Emission spectra of ABDA (λ_{exc} = 380 nm) in the presence of (A) $[Ru(phen)_3]^{2+}$, (B) $[Ru(TAP)_2phen]^{2+}$, (C) **1** and (D) **2** in H_2O before and after 10 s irradiation using a CoolLED pE-2 microscope LED illumination source (470 nm, 100% intensity), at 298 K.

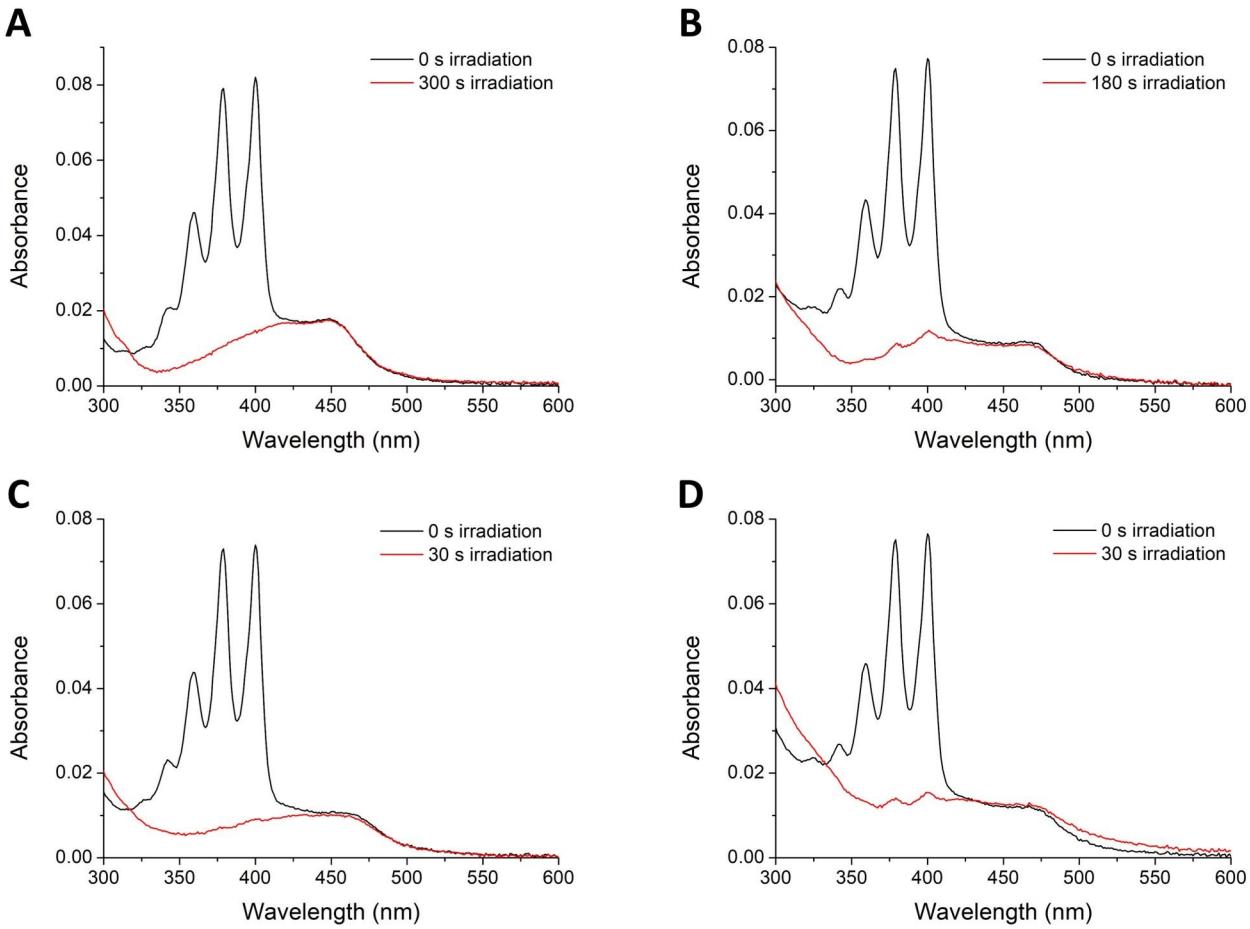

Fig. S18. UV-vis absorption spectra of the solutions containing ABDA and (A) $[Ru(phen)_3]^{2+}$, (B) $[Ru(TAP)_2phen]^{2+}$, (C) **1** and (D) **2** in H_2O before and after irradiation using a CoolLED pE-2 microscope LED illumination source (470 nm, 100% intensity), at 298 K.

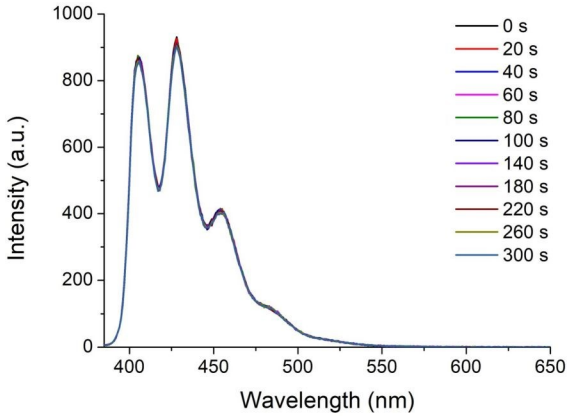

Fig. S19. Emission spectrum of ABDA (λ_{exc} = 380 nm) in the absence of Ru(II) complex in H_2O at different irradiation times using a 470 nm pE-2 LED illumination system (100% intensity), at 298 K.

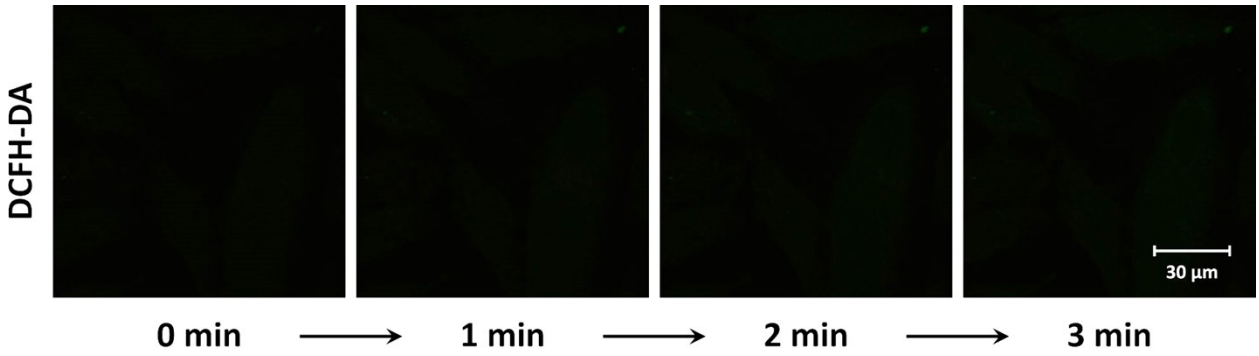

Fig. S20. Confocal fluorescence microscopy images of HeLa cells treated with DCFH-DA (20 μM) before and after irradiation with a 405 nm diode laser for different periods of time showing no ROS generation.